Green Chemistry

PAPER

View Article Online
View Journal | View Issue

Cite this: *Green Chem.*, 2017, **19**, 2406

Mechanism of C–C bond formation in the electrocatalytic reduction of CO_2 to acetic acid. A challenging reaction to use renewable energy with chemistry

Chiara Genovese,* Claudio Ampelli, Siglinda Perathoner* and Gabriele Centi

Received 12th December 2016,
Accepted 2nd March 2017

DOI: 10.1039/c6gc03422e

rsc.li/greenchem

Copper nanoparticles on carbon nanotubes are used in the reduction of CO_2 to acetic acid (with simultaneous water electrolysis) in a flow electrocatalytic reactor operating at room temperature and atmospheric pressure. A turnover frequency of about 7000 h^{-1} and a carbon-based Faradaic selectivity to acetic acid of about 56% were observed, indicating potential interest in this approach for using renewable energy. The only other products of reaction detected were formic acid and methanol (the latter in some cases), besides H_2. The reaction mechanism, particularly the critical step of C–C bond formation, was studied by comparing the reactivity in tests with CO_2 or CO, where formic acid or formaldehyde where initially added. The results indicate the need for having dissolved CO_2 to form acetic acid, likely *via* the reaction of $CO_2^{\bullet-}$ with surface adsorbed $-CH_3$ like species. The pathway towards formic acid is instead different from the route of the formation of acetic acid.

Introduction

Chemical energy storage[1] is a critical factor in pushing for an energy transition together with a larger use of renewable energy, because it addresses the issues towards (i) mitigating the impact of large shares of renewables in the energy mix (due to their intermittency), (ii) using the local potential excess of electrical energy (for example, the wind during the night) and especially (iii) exploiting unused potential sources of renewable energy (hydropower, wind and solar panels in deserts, *etc.*), which cannot be otherwise used due to their remote locations.[2] Although different energy vectors can be used to implement this concept, the products deriving from the reduction of CO_2 play a key role for a better integration into the actual energy and chemical production value chains.[3] The recent white paper on "Solar-driven Chemistry"[4] remarks on how the vision for the future sustainable chemistry will be based around the concepts and technologies for an efficient use of solar energy (direct or indirect uses, *i.e.* the latter through the intermediate production of renewable electrical energy). The electrocatalytic reduction of CO_2, from this perspective, is thus a key area for moving to this novel chemistry. We use here the term electro-catalysis rather than the more common electrochemistry, because the understanding of the (electro)catalytic aspects rather than only those of electrochemical conversion (electron transfer, for example) is likely critical to make significant progress in the control of selectivity in CO_2 reduction.

Although the electrocatalytic reduction of CO_2 has been known for many years,[5] and various reviews have also addressed this topic recently,[6] there is still an open key question with respect to the mechanism of the formation of C–C bonds during the electrocatalytic reduction of CO_2. To produce longer chain chemicals or fuels (*i.e.* >C1) during the electrocatalytic reduction of CO_2 is a great challenge, but rather interesting from the application perspective: better use as drop-in products, better sustainability with respect to the multistep current production. Realizing C–C bond formation during the electrocatalytic reduction, in addition, goes in the direction of multistep integration in (electro)catalytic reactions, one of the challenges to progress to a more sustainable chemistry identified in the recent "Science and Technology Roadmap of Catalysis for Europe".[7]

Cu electrodes exhibit a distinct catalytic ability to produce ethanol and ethylene by electrocatalytic reduction of CO_2, although at relatively high overpotentials where the electrode stability is limited.[8] Earlier works showed that CO is a key intermediate in the formation of hydrocarbons from the reduction of CO_2 on copper.[8d] This hypothesis is now widely accepted in the literature, although the identification of a conclusive mechanism for the reduction of CO_2 on copper is still challenging.[6a] One of the points is also that up to 16 different products were identified to form from CO_2 under these condi-

Univ. Messina and INSTM/CASPE, Industrial Chemistry (Depts MIFT & ChimBioFarAm), V.le F. Stagno D'Alcontres 31-98166, Messina, Italy.
E-mail: cgenovese@unime.it, perathon@unime.it

tions.[8e] Besides methane and ethylene, these products include a broad mix of aldehydes, ketones, carboxylic acids, and alcohols.

Earlier mechanistic studies also indicate that the mechanistic pathway toward formic acid is different from the hydrocarbon pathway, which proceeds through CO intermediate formation that is dissociated on the surface and hydrogenated to form a carbene species ($*CH_2$) on the surface.[8f,g] The latter species may then be further hydrogenated to methane (by reacting with two H^+/e^-) or react with another carbene species to form ethylene. Alternatively, the carbene (in a Fischer–Tropsch-like step) may react with CO to form alcohols.[9] There is no general agreement that this reaction mechanism and types of reaction intermediates is related to C–C bond formation (or in general related to hydrocarbon formation) during the electrocatalytic reduction of CO_2. For example, DFT studies on a Cu(211) surface suggest that in the thermodynamically most favourable pathway (to form methane from CO_2), the second C–O bond is broken only at a late stage of the mechanism.[10] The activated CO species (*CO) is hydrogenated to *HCO, $*H_2CO$, and $*H_3CO$ (methoxy), and this methoxy intermediate is reduced to CH_4 and *O, which is finally reduced to H_2O. Ethylene is formed by dimerization of H_xCO species and subsequent deoxygenation.[11] This mechanism, however, does not explain the experimental evidence that formaldehyde (CH_2O) is reduced only to methanol (CH_3OH) and that methanol cannot be reduced to methane.[12] An alternative theoretical study on Cu(111)[13] indicates a different mechanism for the formation of CH_4, where the formation of C_2H_4 occurs *via* coupling of $*CH_2$ moieties. Koper and coworkers,[6e] analysing all these data, concluded that there are distinct paths to methane and ethylene, observing also that the reaction mechanism is dependent on pH and is structure sensitive. In the first pathway, the CO intermediate is first reduced to a formyl species (*CHO) or a *COH species, which is further reduced to methane. Dimerization of the intermediates in this pathway may also yield ethylene at high applied overpotentials (>10 mA cm^{-2}). However, the preferable path to afford the C–C bond (at low overpotentials) is a CO dimerization step mediated by electron transfer to give a $*C_2O_2^-$ intermediate (rate determining step), followed by proton transfer.[14] On roughened copper-nanoparticle-covered electrodes, the relative selectivity toward ethylene over methane could be increased, likely due to their more defective structure.[15] This type of electrode, as well as those based on copper nanoparticles, show reduced onset potentials for both formic acid and CO and also an increased stability in comparison with polycrystalline copper electrodes,[16] which generally show fast deactivation. The size of Cu nanoparticles is also important. Nanoparticles below about 2 nm show enhanced activity, but only towards H_2 and CO formation, while hydrocarbon formation essentially disappears.[17] A recent work on oxide-derived copper electrodes indicated acetaldehyde (produced with a Faradaic efficiency of about 5%) as the key intermediate in the electroreduction of CO to ethanol.[18] Adsorbed *OCCHO (deriving from the H^+/e^- addition to CO dimer)[14a] is indicated by DFT calculations on Cu(211), as the likely intermediate in the C–C coupling and in the pathway to the final formation of ethanol.

There are thus still contrasting ideas about the key intermediates in C–C bond formation during the electrocatalytic reduction of CO_2. By studying the electrocatalytic behaviour of iron, copper and other metal nanoparticles supported on carbon nanotubes (CNTs) in the reduction of CO_2 under liquid and gas phase conditions (the latter are without the presence of a bulk electrolyte as in all cases of the above cited studies), we observed that on the same electrocatalysts these two reaction conditions lead to different types of products.[19] Hydrocarbons and alcohols up to C3–C4 were detected under gas phase conditions, while acetic acid together with small amounts of few other products were detected under liquid phase conditions, *i.e.* conditions closer to those studied by the other cited authors and used in most of the electrocatalytic studies on the reduction of CO_2. In particular, the electrocatalysts based on copper nanoparticles on CNTs showed a more selective formation of acetic acid, a product which was earlier observed to be always in minor (trace) amounts, with the main products being ethylene and ethanol as >C1 products.

Direct synthesis of acetic acid from CO_2 is an interesting reaction. Some studies have earlier reported on the possibility to directly produce acetic acid from CO_2 and CH_4, particularly on metallo-zeolites, even if mainly based on theoretical studies.[20] For example, Panjan *et al.*[21] have investigated this reaction from a theoretical approach on an Au-exchanged ZSM-5 catalyst. The activation of the C–H bond over the Au-ZSM-5 zeolite would readily take place *via* the homolytic σ-bond activation with an energy barrier of 10.5 kcal mol^{-1}, and the subsequent proton transfer from the Au cation to the zeolitic oxygen, yielding a stable methyl–gold complex adsorbed on the zeolite Brønsted acid. The conversion of CO_2 on this bifunctional catalyst involves the Brønsted acid site playing a role in the protonation of CO_2 and the methyl–gold complex acting as a methylating agent. Wu *et al.*[22] instead investigated the formation of acetic acid from CH_4/CO_2 on zinc-modified H-ZSM-5. They indicated that zinc sites efficiently activate CH_4 to form zinc Me species ($–Zn–CH_3$), the Zn–C bond of which is further subjected to CO_2 insertion to produce surface acetate species. Moreover, the Brønsted acid sites play an important role in the final formation of acetic acid by proton transfer to surface acetate species. In both cases, there is thus the formation of a methyl radical intermediate (likely stabilized by the interaction with the metal and the zeolitic cage), which then reacts with CO_2, likely activated by the interaction with Brønsted acid sites.

There are thus some possible analogies in the reaction mechanism of the electrocatalytic reduction of CO_2, with the CH_x species generated by CH_4 dissociation (in the catalytic conversion), rather than on the electrocatalyst surface as it may occur during the electroreduction of CO_2. A notable difference with respect to the previously mentioned reaction mechanisms is that there is no generation of CO as the first step in the reduction of CO_2 as a prerequisite to form C–C bonds. While those discussed before are somewhat a modification of the reaction mechanisms present in Fischer–Tropsch type reactions,[23] the formation of >C1 products without the formation

of CO as an intermediate (except possibly for the generation of surface CH_x adspecies) should involve a different reaction mechanism.

In terms of moving to the use of renewable energy in chemical production (the solar-driven chemistry concept introduced above), there is a specific interest for the possibility to produce acetic acid directly from CO_2, even with relatively low energy efficiencies. In fact, the current synthesis process of acetic acid is multi-step, *via* the production of syngas from methane, production of methanol, and carbonylation of the latter. The maximum overall energy efficiency, as theoretical minimum process energy (the minimum amount of energy required for the process based on chemical reactions and ideal or standard conditions and 100% yield) divided by the total process energy input is about 27% for acetic acid.[24] The effective energy efficiency is even lower, the yield being less than 100%, but already this value shows how the majority of the energy content in fossil fuel raw materials is lost in the process of the production of chemicals using the current process technologies. Although electrocatalytic processes still suffer today from low productivity and often low selectivity, the above considerations remark how there is an interesting potential, particularly in producing more complex products from a waste such as CO_2. This is quite challenging, but a necessary approach to use renewable energy with chemistry. Understanding all the possibilities in forming the C–C bond in the electrocatalytic reduction of CO_2 is thus a key element from this perspective.

Experimental

Synthesis of the electrode materials

The working electrode for the electrochemical cells for CO_2 reduction consists of a carbon substrate on which the copper metal nanoparticles are deposited. This electrocatalyst is then deposited on a gas diffusion layer (GDL 25 BC Sigracet®), on the side not modified with Teflon. The substrate is carbon nanotubes (CNTs, PR-24-XT-PS Pyrograf®).

PR-24-XT-PS CNTs have an average diameter of about 100 nanometers. The inner part shows well-ordered graphitic layers aligned along the main axis, but the external surface displays a turbographic structure. The CNTs were pyrolyzed at 750 °C to remove polyaromatic hydrocarbons from their surface. Due to the turbographic structure, these CNTs offer a large number of sites for the functionalization of the external surface.

The nature of the functional groups on the carbon surface plays a key role in the catalytic activity of the electrocatalysts. Thus, CNTs were functionalized by direct oxidative treatment in concentrated HNO_3, introducing oxygen functionalities on the carbon surface. In detail, 1 g of CNTs was suspended in 50 ml HNO_3 (65% Sigma Aldrich) and treated in reflux at 100 °C for 3 h, followed by rinsing until a neutral pH, filtering, and drying overnight. Different types of oxygen functionalities were introduced by this treatment. The total quantity and relative distribution can vary as a function of the annealing post-treatment under an inert atmosphere, as shown from synchrotron radiation XPS data.[25] The main properties of the GDL and CNTs were reported earlier.[19]

Before depositing the carbon substrates on the GDL, copper nanoparticles (NPs) were deposited on CNTs by an incipient wetness impregnation method using an ethanolic solution containing a suitable metal precursor [$Cu(NO_3)_2{\cdot}3H_2O$]. After drying at 60 °C for 24 h, the samples were annealed for 2 h at 350 °C and reduced at 400 °C under a slow H_2 flow. The total amount of metal loaded onto the carbon substrate was 10 wt%. This amount was chosen in order to have an amount comparable to the metal loading in the electrocatalysts for PEM fuel cells (usually 10–20 wt%), which corresponds to a small metal loading in the final catalyst (about 0.5 mg cm^{-2}).

The as-prepared carbon substrates with the deposited nanoparticles (Cu10-CNT) were then deposited on the GDL (Cu10-CNT/C) using a similar impregnation in anhydrous ethanol and after joining the GDL with the Nafion® membrane, the samples were tested as working electrodes in the cell described below. The electrode is in contact with the electrolyte solution saturated with CO_2. Before the use, the Nafion® membrane was pre-treated with hydrogen peroxide to eliminate organic impurities and finally activated with H_2SO_4.

Characterization of the electrodes

X-ray diffraction (XRD) analyses were performed by using a D2 Phaser Bruker diffractometer equipped with a Ni β-filtered Cu-Kα radiation source operating at 30 kV and 10 mA. The data were collected at a scanning rate of 0.025° s^{-1} in a 2θ range from 15° to 70°. Diffraction peak identification was performed on the basis of the JCPDS database of reference compounds. The average crystallite size corresponding to (111) peaks of CuO is calculated by Debye–Scherrer's formula as:

$$L = k\lambda/\beta \cos\theta \quad (1)$$

where L is the particle size (nm), k is a constant equal to 0.94, λ is the wavelength of X-ray radiation used (1.541 Å), β is the full-width at half maximum (FWHM) of the peak in radians and θ is the Bragg angle.

Transmission electron microscopy (TEM) images were acquired by using a Philips CM12 microscope (resolution 0.2 nm) with an accelerating voltage of 120 kV.

Raman spectra of CNTs, were collected in a range of 400–3000 cm^{-1} by using a Thermo DXR Raman Spectroscopy equipped with a 532 nm diode-pumped solid state (DPSS) laser. A 50× objective was used for all the measurements and 1 mW of laser power was employed to avoid sample damage.

Electrocatalytic tests

The electrochemical cell, made in Plexiglas® to allow visual inspection, has a three-electrode configuration. The working electrode (about 6 cm^2) is located at the cathode side, at about 0.5 cm from a saturated Ag/AgCl electrode (working as the reference electrode). The potential of CO_2 reduction depends on this distance. The electric contact with the working elec-

trode is maintained with a Pt wire. The counter-electrode is a commercial Pt rod (Amel) immersed in the anode compartment. A potentiostat/galvanostat (Amel mod. 2049A) is employed to supply a constant current/bias between the electrodes.

The anode compartment is physically separated from the cathode side by a proton-conducting membrane (Nafion® 117, Ion Power). A 0.5 M aqueous solution of $KHCO_3$ was used as the electrolyte solution in both the cathode and anode compartments. The volume of the electrolyte solution at the anode was about 7 ml. The electrochemical cell was designed in order to have a large surface area of the electrode and to minimize the electrolyte solution in direct contact with the electrocatalyst. A continuous flow of pure CO_2 (10 ml min^{-1}) was introduced into an external reservoir to saturate the electrolyte solution. This prevents interference from gas bubbles striking the electrode surface in the cathode compartment. The electrolyte solution is continuously circulated between the cathode compartment and the external container by using a peristaltic pump. The total amount of solution (cathode + external container) was 25 ml. The pH of the electrolyte is initially 9, but reduces to 5 in the anode side during the experiments.

The liquid products were analysed by sampling the liquid in the external container and determining the composition of the solution using a Gas Chromatography-Mass Spectrometer (GC-MS Thermo 1310-Tsq 8000 Evo, column Stabilwax) and Ion Chromatography (IC Metrohm 940 Professional, column Metrohm Organic Acids). The gas products were detected by sampling the gaseous stream leaving the external container at regular intervals and analysing using gas-chromatography (GC-TCD Agilent 7890A, column 5A Plot). Before starting the electrocatalytic tests, a Cyclic Voltammetry analysis was conducted on the electrocatalysts, from −2 V to 2 V at 5 mV s^{-1}.

A typical experiment is as follows: after CO_2 pre-adsorption for saturation of the system (typically 30 min), pure CO_2 (10 ml min^{-1}) is flowed for 4 h at the cathode and anode sides. CO_2 gas is also flowed into the anodic compartment in order to remove the O_2 produced during the HER (hydrogen evolution reaction), which can accumulate at the Pt counter electrode increasing the overpotential of the cell.

All the experiments were performed in a galvanostatic mode (−100 mA) at room temperature monitoring the formation of products at regular intervals (typically 1, 3 and 4 hours). Particularly, the experiments in the presence of intermediates of the reaction were conducted by adding to the cathode side an appropriate volume in order to obtain a 10^{-2} M final concentration. Formaldehyde solution (37% in H_2O contains 10–15% of methanol as stabilizer) and formic acid 98% were provided by Sigma Aldrich.

Results

Characterization of the electrocatalyst

The phase composition and crystalline size of the Cu10-CNT electrocatalyst were investigated by XRD and the obtained pattern is reported in Fig. 1. The XRD pattern of pure functionalized CNTs is also shown as a comparison.

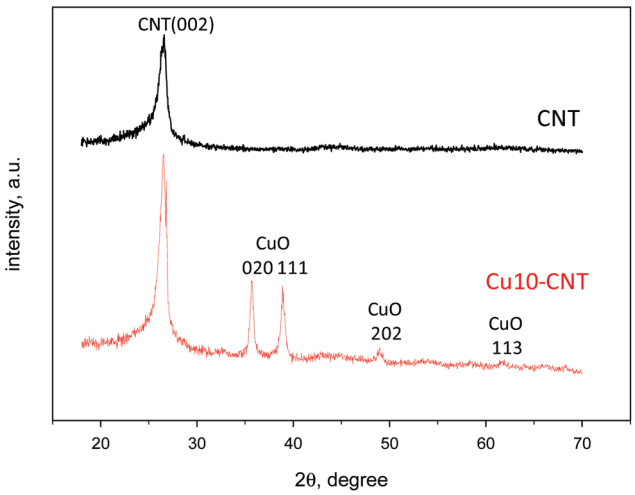

Fig. 1 X-ray diffraction patterns for the Cu10-CNT electrocatalyst and of the parent CNT substrate as a reference.

The dominant diffraction peak at 26.4° can be assigned to the (002) planes of the hexagonal graphite structure of CNTs with an interplanar spacing of 0.34 nm. Two twin peaks at 2θ = 35.67° and 38.90° and a weak peak at 2θ = 48.97° were observed corresponding to the planes (020), (111) and (202) of monoclinic CuO, respectively (JCPDS 80-1916).

The average crystallite size, determined by the Scherrer equation, lies in the range of 38–40 nm. The relative intensity of the diffraction lines for CuO is in agreement with that observed for nanoparticles, without a specific preferential exposure of some crystalline planes.

Transmission electron microscopy (TEM) was used to determine the morphology and the particle size distribution of the Cu10-CNT catalyst. A representative TEM image of Cu10-CNT is shown in Fig. 2. Round-like particles are mainly localized inside the nanotubes with a relatively narrow size distribution. The estimated average particle diameter is 43 nm, which is in good agreement with XRD results.

The Raman spectrum of pure CNTs (reported in Fig. 3) shows two main intense bands centred at 1349 and 1588 cm^{-1} that can be interpreted as an E_{2g} mode of graphite. The G-band (1588 cm^{-1}) is a tangential shear mode of carbon atoms originating from the stretching mode in the graphite plane. The D-band (1349 cm^{-1}) is generally referred to the disorder in the graphite layer and becomes inactive in a perfect ordered structure. In CNTs, the D-band is activated by the presence of vacancies, heteroatoms or other defects in the plane. The intensity ratio between the D and G bands I_D/I_G provides a parameter that indicates the relative degree of graphitization. The stronger the intensity of the D band, the higher is the disorder degree in the graphite layer.[26] The ratio I_D/I_G is equal to 0.75 for CNTs and 0.72 in Cu10-CNT. There is thus a slight decrease of disorder in CNTs upon deposition of copper nanoparticles, as may be expected for a preferential location of the

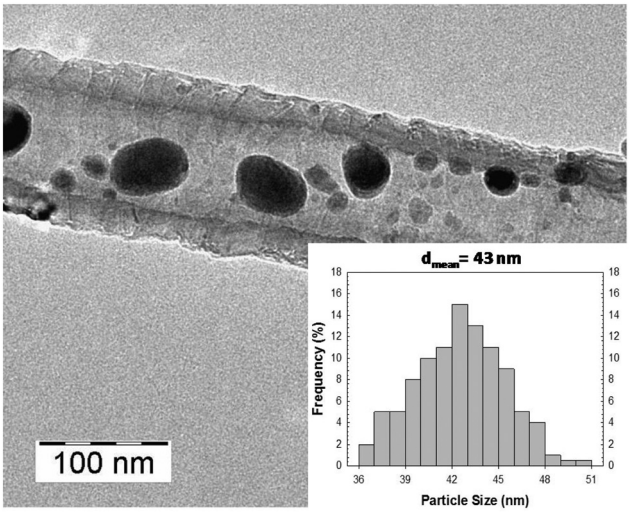

Fig. 2 TEM image of the Cu10-CNT sample with the estimated particle distribution.

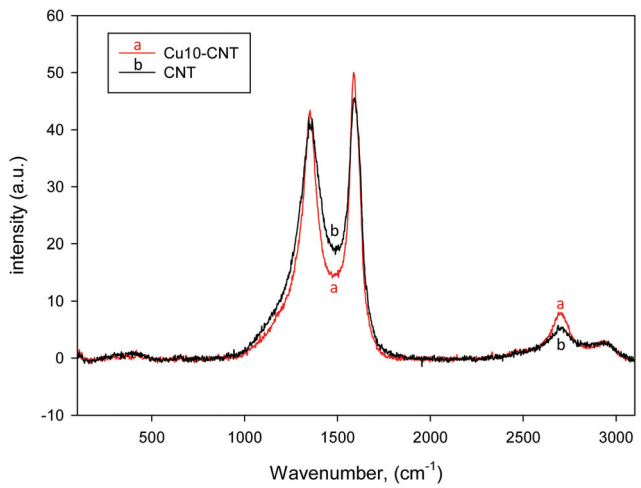

Fig. 3 Raman spectra of pure CNTs and Cu10-CNT samples.

metal nanoparticles on these carbon defect sites. The effect, however, is relatively minor.

Another peak is found at about 2700 cm^{-1} referred to as the G′ band. This is because a second-order (two phonons) Raman scattering from D band variation is characteristic of all the types of CNTs, also defect-free (for which the D-band is not present).[27]

Electrocatalytic tests

Open circuit measurements. The reaction of CO_2 reduction was preliminarily studied under open circuit voltage (OCV) conditions, in order to analyse the background catalytic activity under the chosen utilized reaction conditions. In this case, H_2 (1.5 vol%) was co-fed with CO_2 into the external reservoir directly connected to the cathode compartment, because under electrocatalytic conditions the H_2 equivalent (H^+/e^-) are generated from water electrolysis on the other hemi-cell. This OCV experiment thus provides the basic activity of the electrocatalyst in the absence of any current/voltage applied. Before the OCV experiments, the electrocatalyst was pretreated at a voltage of −1.4 V, in order to have a surface situation closer to that observed in close circuit experiments (see later).

In the OCV experiment, formic acid and acetic acid formation rates of 64.3 and 43.9 μmol h^{-1} $g_{Cu}{}^{-1}$ were observed, respectively, while no methanol was detected, at least within our detection limit (below one μmol L^{-1}). The production rates reported refer to average values in 4 h of reaction. A stable behaviour was observed during this period and beyond, indicating that the products detected were not associated with the desorption from the catalyst of contaminating species. This was verified in blank tests without feeding CO_2, where no products were detected (see later). There is thus a low, but not negligible activity of the catalyst in the absence of applied voltage/current.

Close circuit measurements. For closed circuit conditions, the CO_2 reduction process was carried out following the procedure described in the experimental part. We operated at the galvanostatic mode applying a constant current (negative) at the working electrode (the Nafion®-assembled Cu10-CNT/C) and reading the voltage generated. Before starting the testing experiment, analysis by Cyclic Voltammetry (CV) was made to study the onset voltage of CO_2 reduction on Cu10-CNT/C. Fig. 4 shows the CV profile obtained in the potential interval −2/+2 V (*vs.* Ag/AgCl) at a scan rate of 5 mV s^{-1}.

Two main reduction peaks can be observed at −0.55 and −1.2 V, which can be associated with the changes in the oxidation state of Cu (from Cu^{II} to Cu^{I} and from Cu^{I} to Cu^{0}). At more negative potentials, an onset voltage of about −1.35 V was observed. Even if some products can also be produced at a higher voltage (>−1.35 V), a strong change in productivity was observed under this onset value. Moreover, from an industrial perspective it should be more convenient to operate at rela-

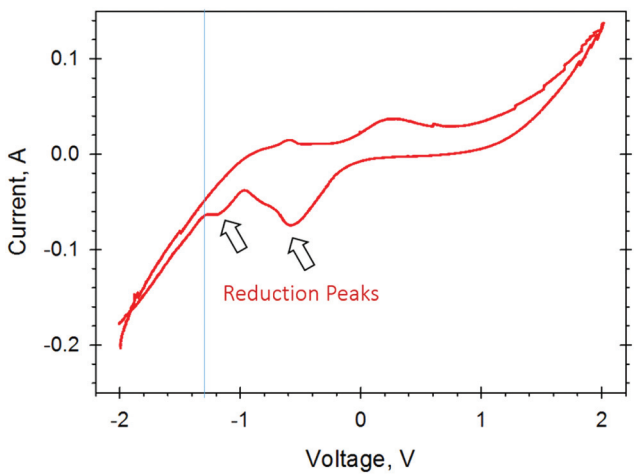

Fig. 4 Cyclic voltammetry (CV) profiles from −2/+2 V (*vs.* Ag/AgCl) at a scan rate of 5 mV s^{-1} on Cu10-CNT/C.

tively high current density to make the process economically feasible.[28] As a result, we operated by applying a constant current of −100 mA in order to obtain −1.4 V of initial bias.

Under these conditions, formic acid and acetic acid form as the main products with rates of 212.7 and 208.7 μmol h^{-1} $g_{Cu}{}^{-1}$, respectively. Methanol was also produced at a rate of 13.6 μmol h^{-1} $g_{Cu}{}^{-1}$. The analysis of the outlet gaseous stream of the continuous electrocatalytic reactor reveals the formation of hydrogen, whose rate of production was 0.321 μmol min^{-1}. CO and CH_4 were not detected in the continuous electrocatalytic reactor outlet gaseous stream.

The observed rates of reaction remain quite constant until 24 h, evidencing a good stability on a laboratory scale. Analysis of the cathodic solution by atomic absorption spectroscopy at the end of the tests did not show the presence of Cu in the electrolyte solution, indicating the absence of copper leaching during the electrocatalytic experiments. With respect to OCV conditions, the reaction rates of formic and acetic acid increase by a factor of about 3.5–4.0, while methanol is also detected. Note that acetic acid, *i.e.* a product involving C–C bond formation, was never detected as one of the main products of the reaction in literature data on the electrocatalytic reduction of CO_2.

We will refer hereinafter to the experimental electrocatalytic test reported above as the reference to which we compare the behaviour using different feeds.

By considering the size distribution of the Cu particles evidenced by TEM measurements (Fig. 2) and the Cu loading (assuming copper hemispheres deposited on the CNT), it is possible to estimate the electrocatalytically active surface area of copper. The turnover frequency (TOF) that can be estimated based on this indication is shown in Table 1 for formic acid, acetic acid and methanol. Good TOF values are observed. As a reference value, Ishitani *et al.*[29] which cited high turnover frequency in the photocatalytic CO_2 reduction with Ru(II) multinuclear complexes, reported a TOF of 696 h^{-1} in formic acid formation.

The carbon-basis Faradaic selectivity, *i.e.* the selectivity in the reduction of CO_2 taking into account that 2, 4 and 6 electrons are necessary to reduce CO_2 to formic acid, acetic acid and methanol, respectively, is also shown in Table 1. Acetic acid with a selectivity close to 60% is formed on the Cu10-CNT electrocatalyst.

The total Faradaic efficiency, *i.e.* by considering that electrons are also used to generate H_2 by water electrolysis (instead of using the protons/electrons to reduce CO_2), however, is lower, about 3% at a voltage of −1.4 V. By decreasing the applied voltage (from −1.4 V to −0.5 V), the Faradaic efficiency to the products of CO_2 reduction strongly increased to about 70%, although at this voltage the current density and thus productivity is quite low. Although the Faradaic efficiency to the products of CO_2 reduction is low at −1.4 V, it is in good agreement with that observed in the literature, as commented on in the Introduction.

Tests in the presence of possible reaction intermediates

With the aim to understand the mechanistic pathway towards the formation of acetic acid, some tests of CO_2 reduction were made in the presence of the possible reaction intermediates, such as formaldehyde, formic acid and methane. Table 2 reports the production rates of formic acid, acetic acid and methanol obtained in these tests. Note that the formaldehyde reagent that we used was stabilized in methanol, thus the methanol production rate reported refers to the additional production. The addition of formic acid (10^{-2} M) did not influence the formation of acetic acid, the latter being produced at 199.9 μmol h^{-1} $g_{Cu}{}^{-1}$ (against 208.7 μmol h^{-1} $g_{Cu}{}^{-1}$ obtained in the electrocatalytic test under standard conditions). A similar consideration can be made for methanol that was produced at a rate of 16.3 μmol h^{-1} $g_{Cu}{}^{-1}$, thus only slightly higher than standard conditions (13.6 μmol h^{-1} $g_{Cu}{}^{-1}$).

Formaldehyde may be one of the intermediates in the reduction of CO_2. Although we did not detect formaldehyde between the reaction products, this may derive from its instability. We have thus analysed the effect of adding small amounts of formaldehyde to the reacting solution. As shown in Table 2, the presence of formaldehyde: (i) strongly inhibits the production rate of acetic acid, (ii) strongly increases (over 18 times) the formic acid production rate and (iii) very strongly increases (almost 60 times) methanol formation with respect to the test under standard conditions. Formaldehyde is thus clearly promoting methanol formation, reasonably being an intermediate in this pathway (water formation was omitted for clarity):

$$CO_2 \xrightarrow{2H^+,2e^-} HCOOH \xrightarrow{2H^+,2e^-} HCHO \xrightarrow{2H^+,2e^-} CH_3OH.$$

However, in this reaction scheme, it is more difficult to explain the increase in formic acid production by the addition of formaldehyde. Although these reactions are reversible in principle, under negative potential it is not likely that the reaction of formaldehyde oxidation (release of two electrons) may occur. The more reasonable interpretation is a competition

Table 1 TOF numbers calculated in molecules per hour and catalytic site (h^{-1}) and carbon-basis Faradaic selectivity on the products of CO_2 reduction

	Formic acid	Acetic acid	Methanol	Total
TOF	9144	7272	720	17 136
Selectivity	35.4	56.3	8.3	100

Table 2 Products obtained from the electrocatalytic reduction of CO_2 on Cu-10-CNT/C in the presence of possible reaction intermediates (HCHO, HCOOH and CH_4)

Reaction	Electrolyte 0.5 M	Formic acid (μmol h^{-1} $g_{Cu}{}^{-1}$)	Acetic acid (μmol h^{-1} $g_{Cu}{}^{-1}$)	Methanol (μmol h^{-1} $g_{Cu}{}^{-1}$)
CO_2	$KHCO_3$	212.7	208.7	13.6
CO_2 + HCOOH	$KHCO_3$	—	199.9	16.3
CO_2 + HCHO	$KHCO_3$	3222.7	18.82	773.1
CO_2 + CH_4	$KHCO_3$	722.2	6.9	1.7

between the species to be adsorbed at the electrode surface, as discussed later.

To evaluate the influence of CH_4 as a possible intermediate towards the production of acetic acid, one test was performed by flowing CH_4 (3 vol%) together with CO_2. As reported in Table 2, there was a higher production rate of formic acid with respect to the test under standard conditions (722.2 *vs.* 212.7 μmol h^{-1} $g_{Cu}{}^{-1}$), but the production rates of acetic acid and methanol decrease. Hydrogen productivity, instead, largely increased (93.7 μmol min^{-1}), probably due to the steam reforming of CH_4.

Finally, an experiment in the presence of Dimethyl Carbonate (DMC) was performed in order to exclude a possible further route toward acetic acid *via* a nucleophilic attack from this typical methylation agent. The addition of DMC (10^{-2} M) did not influence the formation of acetic acid, the latter being produced at a rate of 184.6 μmol h^{-1} $g_{Cu}{}^{-1}$ (against 208.7 μmol h^{-1} $g_{Cu}{}^{-1}$ obtained under standard conditions).

Tests without CO_2

A blank test without CO_2 was performed to evaluate the influence of the C-based support (CNTs and GDL) as a source of carbon. An inert gas (100% N_2) was introduced into the external reservoir directly connected to the cathode compartment to eliminate the oxygen dissolved. The results showed no acetic acid formation, 19.1 μmol h^{-1} $g_{Cu}{}^{-1}$ of formic acid and 118.4 μmol h^{-1} $g_{Cu}{}^{-1}$ of methanol. These values are summarized in Table 3.

The production rate of formic acid was strongly decreased with respect to the electrocatalytic test under standard conditions, while methanol was produced with a rate almost one order of magnitude higher. It may be noted, however, that these products may derive from the electrocatalytic reduction of hydrogen carbonate ions of the $KHCO_3$ electrolyte, according to the acid–base equilibrium:

$$CO_2 + H_2O \rightleftarrows H^+ + HCO_3{}^-. \quad (2)$$

To verify this hypothesis, another blank test was performed replacing the $KHCO_3$ electrolyte with KCl and without flowing CO_2. In this case, no C-products were detected, confirming that the observed formic acid or methanol derived from the reduction of the hydrogen carbonate ions and not from the CNTs or GDL carbon substrates. Note, however, that without the presence of a flux of CO_2, no acetic acid formation was detected. Even if an equilibrium exists between dissolved CO_2 and hydrogen carbonate, as indicated in eqn (2), the amount of dissolved CO_2 at the electrode surface is likely too low in the absence of a flux of CO_2 to allow the acetic acid formation.

The influence of the presence of possible reaction intermediates for the formation of acetic acid and methanol was also evaluated in the absence of a flux of CO_2. The results are reported in Table 3.

In the presence of formic acid or formaldehyde, no acetic acid was produced (except for a low production with formaldehyde, likely due to the $KHCO_3$ electrolyte, as discussed above). This is a clear indication that the dissolved CO_2 is of critical relevance for the synthesis of acetic acid. Furthermore, the presence of formaldehyde leads to an increase in both formic acid (almost 13 times higher than the reaction without CO_2 and formaldehyde) and methanol production (over 18 times higher) rates, evidencing also in this case a strict correlation between formaldehyde and methanol formation.

Tests with CO

Some tests were carried out by replacing CO_2 with CO. This was done to understand the role that CO may have in the mechanistic pathway towards the formation of acetic acid. A flow of CO (5% in He) was introduced into the external reservoir directly connected to the cathode compartment to saturate the electrolyte solution. The addition of formic acid and formaldehyde was also repeated for this series of experiments. In contrast to other works reported in the literature, it is to be noted that CO was not detected between the gas phase products leaving the continuous flow electrocatalytic reactor. The results are summarized in Table 4.

When CO is fluxed to the cathode, formic acid and acetic acid formation rates of 31.6 and 51.7 μmol h^{-1} $g_{Cu}{}^{-1}$ were observed, respectively, while no methanol was detected. Thus, there is a substantial decrease of productivity with respect to the electrocatalytic test under standard conditions. Replacing the $KHCO_3$ electrolyte with KCl, the production of formic acid strongly increased (763.0 μmol h^{-1} $g_{Cu}{}^{-1}$) and no acetic acid was produced, while methanol was detected in small concentrations. The reaction pathway towards the formation of >C1 products is thus different from those reported in the literature,

Table 3 Products obtained from the electrocatalytic process on Cu10-CNT/C in the absence of CO_2 and in the presence of possible reaction intermediates (HCHO, HCOOH)

Reaction	Electrolyte 0.5 M	Formic acid (μmol h^{-1} $g_{Cu}{}^{-1}$)	Acetic acid (μmol h^{-1} $g_{Cu}{}^{-1}$)	Methanol (μmol h^{-1} $g_{Cu}{}^{-1}$)
No CO_2	$KHCO_3$	19.1	0	118.4
No CO_2	KCl	0	0	0
No CO_2 + HCOOH	$KHCO_3$	—	0	8.63
No CO_2 + HCHO	$KHCO_3$	248.0	21.1	2165
No CO_2 + HCHO	KCl	318.8	0	652.0

Table 4 Products obtained from the electrocatalytic process on Cu10-CNT/C replacing CO_2 with CO and in the presence of possible reaction intermediates (HCHO, HCOOH)

Reaction	Electrolyte 0.5 M	Formic acid (μmol h^{-1} $g_{Cu}{}^{-1}$)	Acetic acid (μmol h^{-1} $g_{Cu}{}^{-1}$)	Methanol (μmol h^{-1} $g_{Cu}{}^{-1}$)
CO	$KHCO_3$	31.6	51.7	0
CO	KCl	763.0	0	7.3
CO + HCOOH	$KHCO_3$	0	0	1.91
CO + HCHO	$KHCO_3$	111.7	34.5	1380
CO + HCHO	KCl	332.5	0	2606

which consider CO as the main intermediate in CO_2 reduction, as discussed in Introduction.

The experimental tests in the presence of formic acid and formaldehyde confirm the trend already shown by the previous experiments with or without CO_2.

Discussion

The use of an electrocatalyst based on copper nanoparticles supported over CNTs allows us to synthetize acetic acid from CO_2 with relatively high TOF and carbon-based selectivity. This is a novel reaction. Although some acetic acid was also detected by other authors during the reduction of CO_2, as commented on in the Introduction, only traces were observed and never as one of the main products of conversion. The industrial synthesis of acetic acid is a multistep process starting from typically natural gas, *via* syngas, used to produce methanol that is then converted to acetic acid by carbonylation. With respect to this industrial route, the direct production of acetic acid from CO_2 may be interesting because it (i) uses a low-value (waste) reactant, (ii) uses renewable energy in the electrocatalytic process of CO_2 reduction, (iii) allows potentially a higher energy efficiency. The alternative possibility is a biocatalytic route. LanzaTech announced in 2012 a partnership with Malaysian oil and gas company Petronas to develop a CO_2-to-acetic acid process, based on its gas fermentation technology.[30] The process is likely using acetogens, which is known to reduce CO_2 with H_2 to acetic acid *via* the Wood–Ljungdahl pathway, in which the ATP required for formate activation is regenerated in the acetate kinase reaction.[31] However, there are no indications allowing to compare productivities, costs and process complexity to recover the acetic acid.

Recently, the possibility of a hybrid approach combining an inorganic semiconductor (CdS) with a bacterium biocatalyst (*Moorella thermoacetica*) was shown.[32] The productivity, however, is low, of the order of 0.5 mM per day, under simulated sunlight with light–dark cycles. In addition, a sacrificial reductant (cysteine, *Cys*; 4 equivalents per mole of CO_2 reduced) is necessary. The data shown in Table 1 for the electrocatalytic reduction of CO_2 to acetic acid thus evidence that this route is promising. However, the productivity of the electrode should be improved and especially it should be limited to the side reaction of H_2 formation, which limits the overall Faradaic efficiency in the use of electrical energy, even if H_2 is a valuable product.

Reaction mechanism and the formation of the C–C bond

Fig. 5 shows the scheme of the possible mechanistic pathway for the electrocatalytic production of formic acid, acetic acid and methanol. The experimental evidence suggests that the formation of acetic acid is due to the reaction between the radical anion $CO_2^{\bullet-}$ with the reduced species $-CH_3$ adsorbed on the catalytic surface.

After a first step of reduction with the initial formation of the radical anion $CO_2^{\bullet-}$, the reaction proceeds to the formation of formate. This can occur in principle without the need for a specific catalyst, as the radical anion $CO_2^{\bullet-}$ can be transformed by a subsequent homogeneous or heterogeneous reaction.[33] Thus, the formation of formic acid can derive from the further reduction of $CO_2^{\bullet-}$ not adsorbed at the electrode surface or, alternatively, it is initiated by the formation of a weakly adsorbed $CO_2^{\bullet-}$, followed by proton attack on the carbon atom.

The pathway towards formic acid should be separated from the route of the formation of acetic acid. Mechanistic studies of Kortlever *et al.*[6e] reported that formic acid cannot be reduced to other products thus confirming our hypothesis. Depending on the nature of the electrocatalyst, the radical anion $CO_2^{\bullet-}$ may strongly interact with the electrode surface. Copper catalytic sites may stabilize $CO_2^{\bullet-}$, which can further reduce to more hydrogenated species. After the adsorption of $CO_2^{\bullet-}$, the first C–O bond is broken with the loss of a water molecule. The intermediate –CHO can further reduce at the electrode surface until a $-CH_2OH$ species is formed. It is to be noted that these half-reactions occur in a strong reducing environment, that is the electrons coming from the anode side

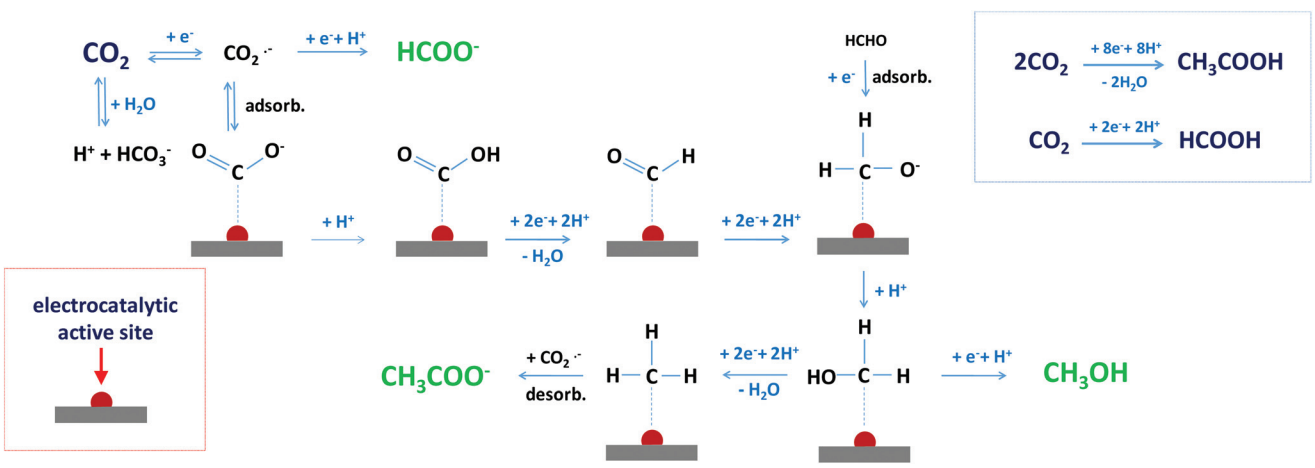

Fig. 5 Schematic mechanistic pathway for the electrocatalytic production of formic acid, acetic acid and methanol on Cu10-CNT/C.

through an external circuit and the protons reaching the cathode from the Nafion® membrane in direct contact with the electrocatalyst.

At this point, the $-CH_2OH$ species may desorb (by a proton attack to the carbon atom from the aqueous solution) to form methanol, or proceed the reduction at the electrode surface. In the last option, the second C–O bond is broken with the loss of another water molecule, with the formation of the adsorbed $-CH_3$ species. This intermediate can be considered as the precursor for the formation of acetic acid. Due to the high concentration of $CO_2^{\bullet-}$ (we operate with 100% CO_2 flow), the adsorbed $-CH_3$ species can undergo a nucleophilic attack from the not adsorbed $CO_2^{\bullet-}$, with the subsequent formation of acetic acid. Alternatively, the adsorbed $-CH_3$ species can combine with $CO_2^{\bullet-}$ adsorbed at a close catalytic site ($-COO^-$) with subsequent formation of acetic acid.

This tentative mechanistic pathway is able to explain most experimental observations that we obtained in our electrocatalytic tests. The introduction of formic acid does not produce an increase in the other reduction products, thus confirming that its formation is different from the specific half-reactions occurring on the electrode surface for the formation of methanol and acetic acid. The reaction in the presence of formaldehyde, however, leads to a strong increase in the production of both methanol and formic acid, but not acetic acid. Formaldehyde is not a stable molecule and tends to adsorb very easily on the electrocatalytic sites. We can suggest that the adsorption of formaldehyde is preceded by the formation of an intermediate species $H_2CO^{\bullet-}$ (similar to $CO_2^{\bullet-}$) that is unstable and compete with $CO_2^{\bullet-}$ for the adsorption at the electrode surface. The more favourable adsorption of formaldehyde leads to the formation of methanol, while $CO_2^{\bullet-}$ does not adsorb at the electrode surface and can only react in the liquid phase with protons to produce a higher quantity of formic acid with respect to the test under standard conditions. For the same reason, the reaction in the presence of formaldehyde proceeds better towards the formation of methanol instead of acetic acid because all the catalytic sites are occupied with formaldehyde and there are no available sites for the adsorption of $CO_2^{\bullet-}$. This can confirm that the production of acetic acid occurs for the combination of two adjacent adsorbed species $-CH_3$ and $-COO^-$. An alternative pathway toward the formation of acetic acid might be the reaction of methanol carbonylation (CO + CH_3OH) but (i) the catalytic systems for this reaction are very different, (ii) we did not observe CO production from the outlet gas stream and (iii) we did not obtain an increased production of acetic acid in the experiments with formaldehyde in the presence of CO.

Furthermore, the electrocatalytic tests without CO_2 produce much less acetic acid, as $CO_2^{\bullet-}$ can be formed only in small concentration due to the presence of the electrolyte $KHCO_3$ (in equilibrium with CO_2, see eqn (2)). If $KHCO_3$ is replaced with KCl, acetic acid formation becomes close to zero, confirming our hypothesis.

The production of acetic acid can be related to the concentration of CO_2 in the cathode compartment. Koleli *et al.*[34] reported a high Faradaic efficiency in the formation of acetic acid on polyaniline electrode in a membrane cell for the electrochemical reduction of CO_2, but they operated under high pressure to increase the solubility of CO_2. We operate at ambient pressure, but we used a pure flow of CO_2 (100%), except for the tests in the presence of reaction intermediates. The production of acetic acid can be ascribed to the high concentration of CO_2, with the subsequent high formation of $CO_2^{\bullet-}$ on the cathode, which can adsorb at the electrode surface and react with the adsorbed reduced species $-CH_3$ giving a molecule of acetate.

Acknowledgements

The financial support of the PRIN 2015 project "Solar driven chemistry: new materials for photo- and electro-catalysis – 2015 K7FZLH" is gratefully acknowledged.

References

1 (*a*) R. Schlögl, *Chemical Energy Storage*, De Gruyter, Berlin, Germany, 2013; (*b*) R. Schlögl, *Green*, 2013, **2**, 233.
2 (*a*) G. Centi and S. Perathoner, *Green Carbon Dioxide: Advances in CO_2 Utilization*, Wiley & Sons, Ny, 2014; (*b*) S. Abate, G. Centi and S. Perathoner, *Green*, 2015, **5**, 43.
3 (*a*) G. Centi, E. A. Quadrelli and S. Perathoner, *Energy Environ. Sci.*, 2013, **6**, 1711; (*b*) C. Ampelli, S. Perathoner and G. Centi, *Philos. Trans. R. Soc. London, Ser., A*, 2015, **373**, 20140177; (*c*) S. Perathoner and G. Centi, *ChemSusChem*, 2014, **7**, 1274.
4 EuCheMS (The European Federation of Catalysis Societies), White Paper on Solar-driven Chemistry, EuCheMS, Bruxelles 2016. Accessible at: http: //www.euchems.eu/solar-driven-chemistry.
5 Y. Hori, in *Modern Aspects of Electrochemistry*, ed. C. G. Vayenas, R. E. White and M. E. Gamboa-Aldeco, Springer, Ny, 2008, vol. 42, p. 89.
6 (*a*) J.-P. Jones, G. K. S. Prakash and G. A. Olah, *Isr. J. Chem.*, 2014, **54**, 1451; (*b*) W.-H. Wang, Y. Himeda, J. T. Muckerman, G. F. Manbeck and E. Fujita, *Chem. Rev.*, 2015, **115**, 12936; (*c*) B. Kumar, J. P. Brian, V. Atla, S. Kumari, K. A. Bertram, R. T. White and J. M. Spurgeon, *Catal. Today*, 2016, **270**, 19; (*d*) Q. Lu and F. Jiao, *Nano Energy*, 2016, **29**, 439; (*e*) R. Kortlever, J. Shen, K. s. J. P. Schouten, F. Calle-Vallejo and M.-T. M. Koper, *J. Phys. Chem. Lett.*, 2015, **6**, 4073; (*f*) M. Gattrell, N. Gupta and A. A. Co, *J. Electroanal. Chem.*, 2006, **594**, 1.
7 European Research Institute of Catalysis (ERIC), *Science and Technology Roadmap of Catalysis for Europe. A Path to create a Sustainable Future*, ERIC Pub., 2016, (ISBN: 979-12-200-1453-3).
8 (*a*) K. P. Kuhl, T. Hatsukade, E. R. Cave, D. N. Abram, J. Kibsgaard and T. F. Jaramillo, *J. Am. Chem. Soc.*, 2014, **136**, 14107; (*b*) F. S. Roberts, K. P. Kuhl and A. Nilsson,

Angew. Chem., In.t Ed., 2015, **54**, 5179; (*c*) Y. Hori, K. Kikuchi and S. Suzuki, *Chem. Lett.*, 1985, **11**, 1695; (*d*) Y. Hori, A. Murata, R. Takahashi and S. Suzuki, *J. Am. Chem. Soc.*, 1987, **109**, 5022; (*e*) K. P. Kuhl, E. R. Cave, D. N. Abram and T. F. Jaramillo, *Energy Environ. Sci.*, 2012, **5**, 7050; (*f*) Y. Hori, A. Murata and R. Takahashi, *J. Chem. Soc., Faraday Trans. 1*, 1989, **85**, 2309; (*g*) R. L. Cook, R. C. MacDuff and A. F. Sammells, *J. Electrochem. Soc.*, 1989, **136**, 1982.

9 Y. Hori, R. Takahashi, Y. Yoshinami and A. Murata, *J. Phys. Chem. B*, 1997, **101**, 7075.

10 A. A. Peterson, F. Abild-Pedersen, F. Studt, J. Rossmeisl and J. K. Norskov, *Energy Environ. Sci.*, 2010, **3**, 1311.

11 J. H. Montoya, A. A. Peterson and J. K. Norskov, *ChemCatChem*, 2013, **5**, 737.

12 K. J. P. Schouten, Y. Kwon, C. J. M. van der Ham, Z. Qin and M. T. M. Koper, *Chem. Sci.*, 2011, **2**, 1902.

13 X. Nie, M. R. Esopi, M. J. Janik and A. Asthagiri, *Angew. Chem., Int. Ed.*, 2013, **52**, 2459.

14 (*a*) F. Calle-Vallejo and M. T. M. Koper, *Angew. Chem., Int. Ed.*, 2013, **52**, 7282; (*b*) J. H. Montoya, C. Shi, K. Chan and J. K. Norskov, *J. Phys. Chem. Lett.*, 2015, **6**, 2032.

15 (*a*) W. Tang, A. A. Peterson, A. S. Varela, Z. P. Jovanov, L. Bech, W. J. Durand, S. Dahl, J. K. Norskov and I. Chorkendorff, *Phys. Chem. Chem. Phys.*, 2012, **14**, 76–81; (*b*) C. S. Chen, A. D. Handoko, J. H. Wan, L. Ma, D. Ren and B. S. Yeo, *Catal. Sci. Technol.*, 2015, **5**, 161.

16 (*a*) C. W. Li and M. W. Kanan, *J. Am. Chem. Soc.*, 2012, **134**, 7231; (*b*) C. W. Li, J. Ciston and M. W. Kanan, *Nature*, 2014, **508**, 504; (*c*) J. Qiao, P. Jiang, J. Liu and J. Zhang, *Electrochem. Commun.*, 2014, **38**, 8.

17 R. Reske, H. Mistry, F. Behafarid, B. Roldan Cuenya and P. Strasser, *J. Am. Chem. Soc.*, 2014, **136**, 6978.

18 A. Verdaguer Casadevall, D. Ravasio, J. H. Montoya, D. B. Trimarco, C. Roy, S. Meier, J. Wendland, J. K. Nørskov, I. E. L. Stephens and I. Chorkendorff, *Angew. Chem., Int. Ed.*, 2016, **55**, 1450.

19 C. Ampelli, C. Genovese, B. C. Marepally, G. Papanikolaou, S. Perathoner and G. Centi, *Faraday Discuss.*, 2015, **183**, 125.

20 S. Abate, K. Barbera, G. Centi, P. Lanzafame and S. Perathoner, *Catal. Sci. Technol.*, 2016, **6**, 248.

21 W. Panjan, J. Sirijaraensre, C. Warakulwit, P. Pantu and J. Limtrakul, *Phys. Chem. Chem. Phys.*, 2012, **14**, 16588.

22 J.-F. Wu, S.-M. Yu, W. D. Wang, Y.-X. Fan, S. Bai, C.-W. Zhang, Q. Gao, J. Huang and W. Wang, *J. Am. Chem. Soc.*, 2013, **135**, 13567.

23 R. A. van Santen, A. J. Markvoort, I. A. W. Filot, M. M. Ghouri and E. J. M. Hensen, *Phys. Chem. Chem. Phys.*, 2013, **15**, 17038.

24 U.S. Department of Energy, *Exergy Analysis: A Powerful Tool for Identifying Process Inefficiencies in the U.S. Chemical Industry*, 2004.

25 C. Genovese, C. Ampelli, S. Perathoner and G. Centi, *J. Energy Chem.*, 2013, **22**, 202.

26 F. Tuinstra and J. L. Koenig, *J. Chem. Phys.*, 1970, **53**, 1126.

27 R. J. Nemanich and S. A. Solin, *Phys. Rev. B: Condens. Matter*, 1979, **20**, 392.

28 C. Oloman and H. Li, *ChemSusChem*, 2008, **1**, 385–391.

29 Y. Tamaki, T. Morimoto, K. Koike and O. Ishitani, *Proc. Natl. Acad. Sci. U. S. A.*, 2012, **109**, 15673–15678.

30 News, Hydroc. Proc., 2012, 15 October.

31 J. Mock, Y. Zheng, R. K. Thauer, A. P. Mueller, S. Ly, L. Tran, S. Segovia, S. Nagaraju, M. Kopke and P. Durre, *J. Bacteriol.*, 2015, **197**, 2965–2680.

32 K. K. Sakimoto, A. B. Wong and P. Yang, *Science*, 2016, **351**, 74–77.

33 Y. Hori, H. Wakebe, T. Tsukamoto and O. Koga, *Electrochim. Acta*, 1994, **39**, 1833.

34 F. Koleli, T. Ropke and C. H. Hamann, *Synth. Met.*, 2004, **140**, 65.